Molecular Dynamics Simulations of Supercritical Jets

Phase III - Item 0002

DLR-LA-MD-RP-006

H. Shin, N. Hammou, G. Schneider,

M. Oschwald

Issue: 1

Lampoldshausen, April 2005 Date: 30.04.2005

Contractor: European Office of Aerospace Research and Development

Contract No.: F61775-01-C0010, Project No. 01-4067

Interim Report Phase III - Item 0002

principal investigator: Michael Oschwald, DLR Lampoldshausen

in cooperation with: Mike M. Micci, The Pennsylvania State University

Dieser Bericht enthält

20 Seiten

18 Bilder

2 Tabellen

6 Literaturstellen

DLR e.V., Institute of Space Propulsion, Lampoldshausen

Report Documentation Page

Form Approved
OMB No. 0704-0188

1. REPORT DATE	2. REPORT TYPE	3. DATES COVERED
19 OCT 2004	**N/A**	**-**

4. TITLE AND SUBTITLE	5a. CONTRACT NUMBER
Molecular Dynamics Simulation of Supercritical Jets	5b. GRANT NUMBER
	5c. PROGRAM ELEMENT NUMBER
6. AUTHOR(S)	5d. PROJECT NUMBER
	5e. TASK NUMBER
	5f. WORK UNIT NUMBER
7. PERFORMING ORGANIZATION NAME(S) AND ADDRESS(ES) **German Aerospace Center DLR Langer Grund Hardthausen D-74239 Germany**	8. PERFORMING ORGANIZATION REPORT NUMBER
9. SPONSORING/MONITORING AGENCY NAME(S) AND ADDRESS(ES)	10. SPONSOR/MONITOR'S ACRONYM(S)
	11. SPONSOR/MONITOR'S REPORT NUMBER(S)

12. DISTRIBUTION/AVAILABILITY STATEMENT
Approved for public release, distribution unlimited

13. SUPPLEMENTARY NOTES
The original document contains color images.

14. ABSTRACT

15. SUBJECT TERMS

16. SECURITY CLASSIFICATION OF:			17. LIMITATION OF ABSTRACT	18. NUMBER OF PAGES	19a. NAME OF RESPONSIBLE PERSON
a. REPORT	b. ABSTRACT	c. THIS PAGE			
unclassified	**unclassified**	**unclassified**	**UU**	**20**	

Table of Contents

1. Experimental Investigation of Laminar Jets in the Sub- and Transcritical Pressure Region

1.1 High speed photography of laminar jets

At the M51 test facility liquid nitrogen is injected at sub- and supercritical pressure at low Reynolds number flow conditions. In the last report [1] the nitrogen jet injection and atomization behavior has been presented based on images recorded at various test conditions (see Table 1).

To resolve the dynamics of the injection process high-speed visualization has been applied. The LN2-jet was back-illuminated by a nanolight and imaged with a CCD-camera with a resolution of 1024x512 pixel and 1KHz frame rate.

High-speed films of the test conditions listed below in Table 1 are attached to this report on a CD.

The films allow to extract information on the jet velocity as well as on the growth of disturbances. Three film stills for test case 3, 3ms, 10ms, and 19ms after starting the recording of the injection process are shown in Figure 1. Clearly two features can be observed:

(i) the jet diameter decreases downstream due the acceleration in the gravitational field

(ii) the liquid surface becomes instable, local variations in the jet diameter increase downstream and result in jet break-up droplet formation.

Exemplary data reductions to quantify these processes are presented in chapter 1.2 and chapter 1.3.

test case	file name	chamber pressure [bar]	reduced pressure $P_r=P/P_C$	total N2-mass flow [g/s]	injector N2-mass flow [mg/s]	injector inner temperature T3 [K]	Re-number of laminar jet
2	02_08_01_05	19.5	0.57	36.5	14.0	99.3	180
3	03_28_01_05	19.5	0.57	54.6	33.6	99.6	388
4	04_28_01_05	25.2	0.74	56.6	35.4	99.5	401
5	05_28_01_05	24.5	0.72	33.7	12.1	101.6	147
6	06_28_01_05	30.3	0.89	33.7	37.9	95.6	379
7	07_28_01_05	30.2	0.89	33.3	12.3	106	171
8	08_28_01_05	39.0	1.15	26.6	2.6	112.7	43
9	09_28_01_05	33.2	0.98	33.6	12.6	104.8	164
10	10_28_01_05	33.1	0.97	72.7	48.2	99.4	533

Table 1: Test conditions

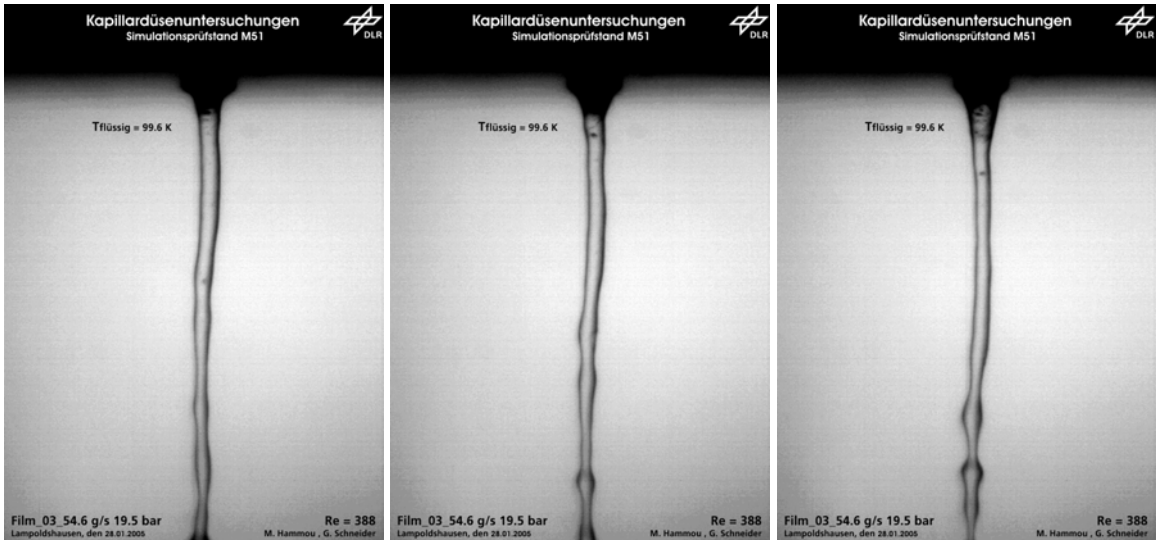

#3 #10 #19

Figure 1: Three film-stills of test case 3.

1.2 Jet diameter

A simple model is used to predict the decrease of the jet diameter of the falling nitrogen jet. The liquid N_2-jet leaving the nozzle with a diameter d_0 and a velocity v_0 is accelerated in the gravitational field. A sketch of the situation is shown in Figure 2. As a consequence of the continuum equation

Eq. 1 $$\rho v \pi \frac{d^2}{4} = const.$$

an increase in v is accompanied by a reduction of the jet diameter d. In the film there is no hint for significant evaporation of the jet, which would appear as schlieren in the images. Thus it is assumed, that the variation of the jet diameter is fully controlled by the gravitational acceleration. The disturbance of the liquid jet surface by instabilities due to surface tension is not taken in into account for the moment.

From the conservation of energy

Eq. 2 $$\rho g h_0 + \frac{\rho}{2} v_0^2 = \rho g h + \frac{\rho}{2} v^2$$

and the continuity equation easily an expression for the variation of the jet diameter with increasing distance x from the nozzle exit can be derived:

Eq. 3 $$d = d_0 \frac{\sqrt{v_0}}{\sqrt[4]{v_0^2 + 2gx}}$$

There is one point to be discussed in respect to an appropriate choice of the initial jet diameter. At first hand one would identify the initial jet diameter with the inner diameter of LN_2-nozzle (see Figure 2a). But there is indication form the images that the surface tension of the liquid nitrogen jet results in a wetting of the LN_2-nozzle front area as shown in Figure 2b. For the evaluation of Eq. 3 the exit velocity v_0 has been calculated from the measured mass flow and the density of nitrogen at the temperature and pressure conditions of the test case. For test case 3 the exit velocity is v_0=0.0312m/s and v_0=0.0153m/s assuming cross sections corresponding to the inner and outer nozzle diameter respectively. Predictions of the jet diameter based on Eq. 3 are shown in Figure 3.

From the high-speed film the jet diameter for test case 3 has been evaluated by image processing methods. The results for frames 3, 10, and 19 are compared to the predictions of the simple model in Figure 3.

The measured diameters near to the nozzle exit are clearly in favor for the assumption of a wetted nozzle front area as sketched in Figure 2b. Further downstream however the model predictions show neglecting differences between assuming wetted and non-wetted nozzle front area.

The experimental data show a significantly smaller decrease of the jet diameter as expected for a jet falling under pure gravity force. A good agreement of model and experiment would be obtained for an assumed injection velocity 1.87 times above the value derived from the mass flow measurement (red dotted line in Figure 3). This is much to large to be explained by mass flow measurement errors.

An increase of the fluid temperature in the nozzle would result in an expansion of the fluid and an acceleration of the flow. Assuming a temperature increase of the jet up to the boiling temperature this would result in a velocity increase of a factor 1.2, again not sufficient to explain the observation. Thus there have to be other factors that systematically increase the velocity of the jet or increase its diameter.

One candidate for an explanation are spots that have been observed in the liquid nitrogen jet. These spots are interpreted as bubbles of gasified N_2. A small amount of gasified LN_2 in the jet at its boiling temperature could easily explain the observed value of the jet diameter. Another hypothesis would be that the drag of the surrounding gas on the jet could partially balance the gravity force. However, we have to admit, that we are not able to give a confirmed explanation for the experimental results.

The experimentally determined jet contours in Figure 3 clearly show that the jet surface becomes unstable due surface tension force. The jet boundary exhibits a wave like contour with growing wave amplitude and decreasing wavelength downstream.

The jet contours of all images of test case 3 for a period of 20ms is shown in Figure 4. The evolution of the surface waves, their growth and their downstream movement can be seen nicely in the waterfall diagram .

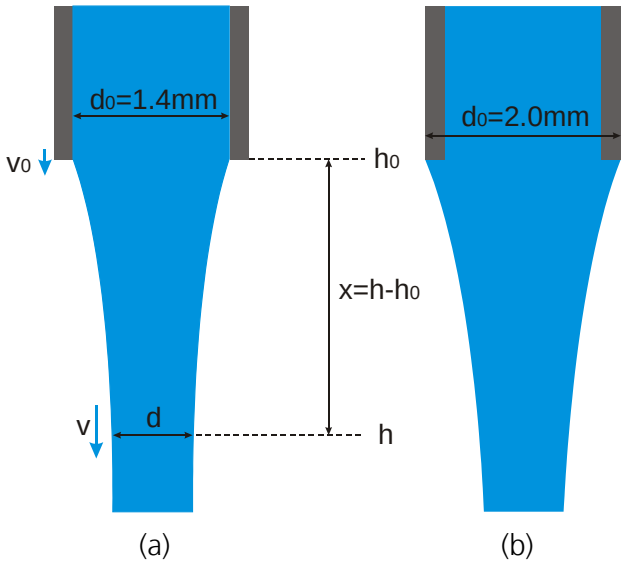

Figure 2: Convergent jet due to acceleration in the gravitational field, (a) without wetting the LN2-post, (b) with wetting the LN2-post

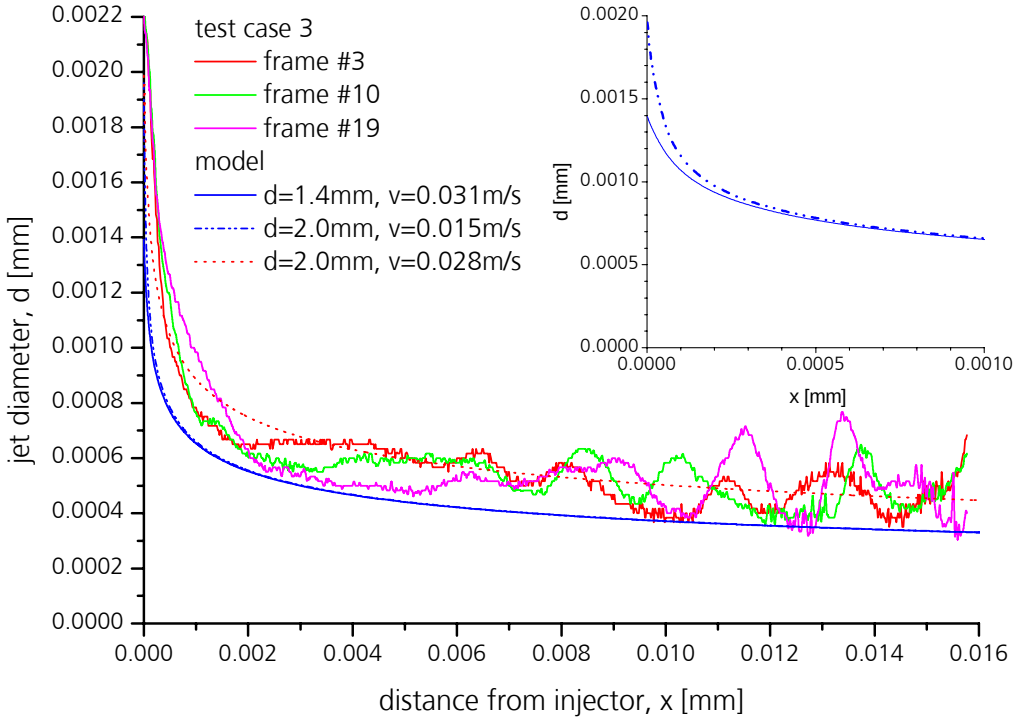

Figure 3: Jet diameter of test case 3. Measured values for frames 3, 10, and 19. Predictions from Eq. 3 without and with wetting of the LN_2-post front area.

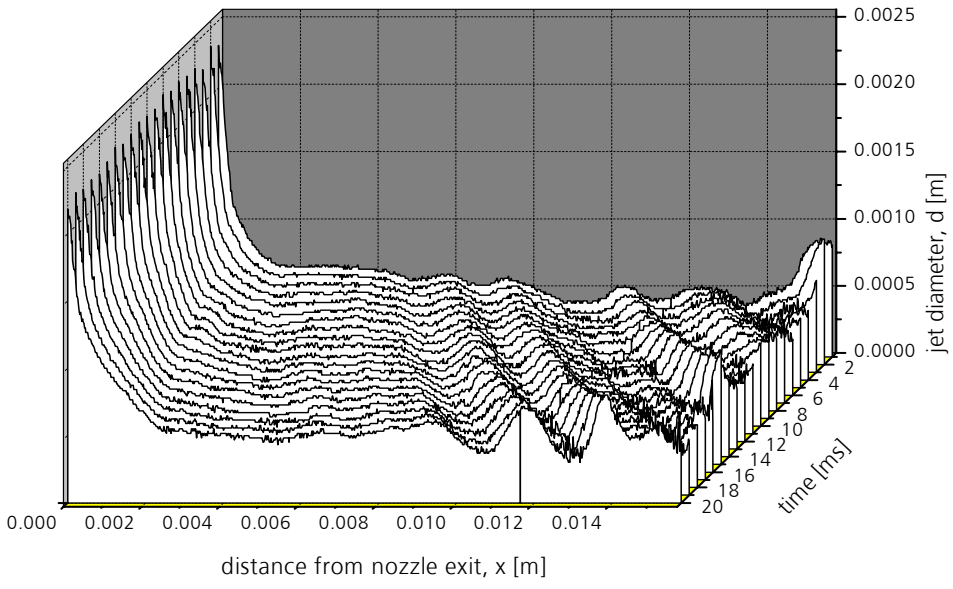

Figure 4: Temporal evolution of the jet diameter for test case 3.

1.3 Jet velocity

In the laminar LN_2-jets dark spots can be observed, an example is shown Figure 5a. These spots are assumed to be gaseous N_2-bubbles, moving inside the liquid N_2-jet.

For test case 3 the position of such a bubble has been determined by visual inspection and by evaluating the bubbles center. This procedure has limited accuracy, due to the difficulty of the visual positioning of a cursor in the center of the bubble. The drag a bubble is exposed to in a moving fluid is significantly higher than the buoyancy forces, therefore the bubble velocity should be identical to the fluid velocity.

The bubble velocity and the velocity of a falling jet as derived from Eq. 2 are shown in Figure 5b. With increasing distance from the injector the bubble velocity becomes more and more smaller than the predicted value for the jet velocity. This would be in coherence with an assumed drag of the surrounding gas on the liquid jet.

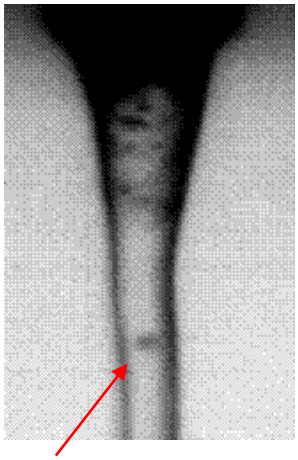

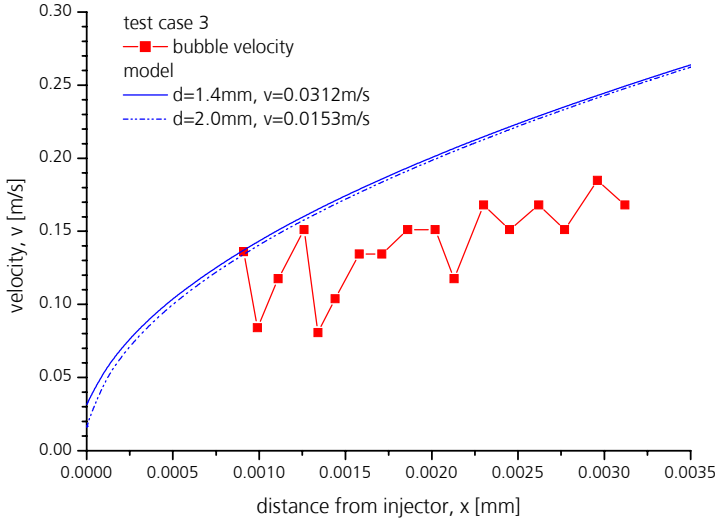

(a) test case 3, frame #3 (b) bubble velocity

Figure 5: (a) bubble in the N_2-jet, (b) bubble velocity

1.4 Concluding Remarks

After modifying the experimental set-up it was possible to realize laminar LN2-jets with Reynolds numbers as small as $\mathbf{Re}$=43. The jets have been investigated at reduced pressures P_r and temperatures T_r with $0.044<P_r<1.15$ and $0.75<T_r<0.89$.

These low Reynolds number flows have low momentum and are therefore very sensitive to disturbances by secondary flows induced in the flow channel. For that reason the jets axis is not stationary but is moving in radial direction. This prohibits measurement techniques that require long data acquisition rates. Especially density measurements by Raman scattering using cw-lasers would deliver density profiles that are smeared out due to the jet movement. For that reason the laminar jets have been analyzed by photography and high speed visualization.

Details of the jet characteristics and its dependence on the flow conditions have been shown in the last report [1]. Generally the well known transition from jet disintegration into droplets at subcritical pressure to mixing of a dense gas into the surrounding gas at supercritical pressure is observed. Increase of the Reynolds number results essentially in an increase of the intact core length.

There is indication from visual observations and evaluation of the jet-diameter in the high-speed films that the LN_2-jets - although injected at temperatures below the boiling temperature - may contain bubbles of gaseous N_2.

The flow velocities derived from the high speed film are clearly below the injection velocities as calculated based on the measured mass flows. As a possible reason for this the drag of the surrounding gas on the liquid jet has been identified.

2. Molecular Dynamics Simulation of Nano-Jets

2.1 Introduction

In previous report, we have presented the argon nanojet injection simulation results under vacuum condition. This study also focused on the effect of injector shape on jet breakup behavior. However, geometrical effects were not so prominent. After a thorough analysis, we concluded that the temperature of the liquid in the solid injector is the governing factor for subsequent nanojet breakup characteristics. We will introduce this conclusion with detailed description in the following section. In addition, the previous nanojet injection code was modified for injection under sub/supercritical pressure. These results will be presented later in this report.

2.2 Liquid – solid phase transition inside the solid injector

Comparing with previous nanojet injection results, two additional properties were newly measured and plotted with 2-D figures. These properties are local pressure and local potential energy. These properties are essential to examine the occurrence of phase transition due to very high pressure. The current jet injection method is 'pressurized injection' therefore we need very high injection pressure to reach the desired level of injection speed. Moreover, the diameter of the injector is only 3 nm and injection speed is an order of 10^2 m/sec. Such a severe injection condition causes significant surface friction and finally leads to drastic injection pressure increase. In our cases, the measured average pressure of jet in the cylindrical injector region is about 500 MPa. This level of pressure was also reported in previous pressurized injection simulation from Micheal Moseler and Uzi Landman [2]. With convergent injector, measured pressure is even higher than that from cylindrical injector. Such a high pressure may cause a phase transition from liquid to solid even with slight higher temperature [3]. The phase diagram of bulk argon in Figure 6 clearly shows the increase of melting point of argon in the very high pressure range. In very high pressure region (above 100 MPa), the melting point of argon is increasing substantially. The zoom in Figure 6-(b) shows that the melting point of argon at 500 MPa is about 180 K which is even higher than its critical temperature (T_c = 150 K).

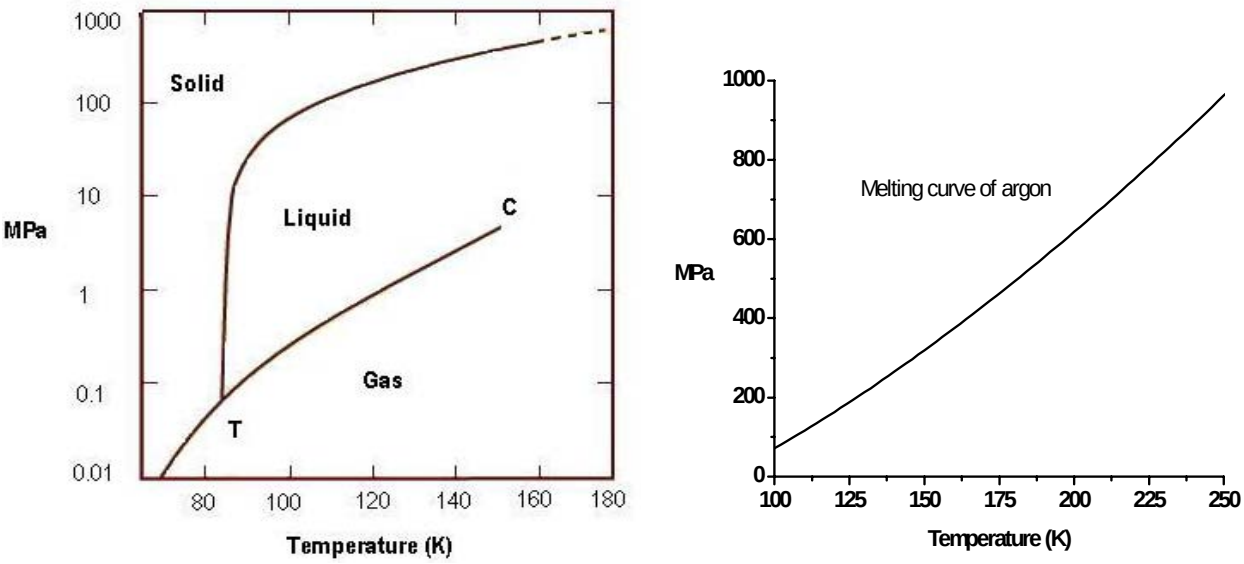

(a) (b)

Figure 6: Phase diagram of argon in low (a) and high pressure range (b).

We are currently dealing with nano-sized system so physical deviations from bulk fluid properties may exist. However, if we assume that this deviation is only marginal, liquid-solid transition can occur

during current simulation due to very high pressure. This phase transition behavior was also reported in water in carbon nanotubes [4][5].

Water in carbon nanotubes can be frozen even at higher temperatures than the normal melting point of water. This behavior strongly depends on the diameter of the carbon nanotubes. Considering that we are using a solid nano-injector which has similar shape and size comparing to carbon nanotubes, this abnormal behavior of liquid in the nano-sized solid tube can exist in our cases.

Therefore, we should keep in mind that liquid can be frozen even in higher temperature than its normal melting point due to too high pressure and nano-sized solid injector.

2.3 Temperature effect on subsequent jet breakup

A series of calculations with various initial thermodynamic conditions have been made to examine the occurrence of liquid-solid transition and the contribution of thermal condition to jet breakup behavior. Three different temperatures were tested with previous cylindrical injector. 2D and 3D plots after 88.21 non-dimensional times are shown in Figure 7. Tested liquid and solid temperatures are 0.93, 1.02, 1.30 (T^*_{liquid}) and 0.94, 1.25, 1.83 (T^*_{solid}) respectively. These temperatures are normalized and one normalized temperature is approximately equal to 120 K. In Figure 7-(a) and (c), average potential energy and axial velocity plots were compared. Relatively small temperature difference causes completely different jet disintegration behavior. In case of the lowest temperature condition ($T^*=0.93$), strong negative potential energy region at the jet core lasts even after injection with slowest injection velocity. In the 3D scatter plot, the difference is more distinct. The general shape of injected jet with lower temperature (Figure 7-(c-3)) is like a frozen jet. Also, vaporized argon atoms are hardly detected in lower temperature case. All these phenomena can be simply explained by the occurrence of liquid-solid phase transition.

Near the inlet of the solid injector, all three cases show solid-like characteristics. Lower level of potential energy, flat axial velocity profiles in this region are evidences of solid state. But, as the jet is moving downstream, the fast pressure drop near the injector exit causes melting of the frozen jet only if the temperature is high enough. Energy conversion from kinetic energy to potential energy is also accompanied with this phase transition. The surplus of kinetic energy from frozen jet should be large enough to initialize solid-liquid phase transition by increasing the level of potential energy. If not, subsequent jet has too low level of potential energy to maintain stable liquid state. Figure 8 shows the jet breakup process with 45 degree injector with slightly elevated temperature. Comparing to results in previous report, only temperature is increased to 1.83 (solid) and 1.4 (liquid). This increase of temperature leads to faster and energetic jet breakup. This result emphasizes that small difference in temperature cause a huge difference in nanojet breakup behavior. Therefore, target temperature in current jet injection simulation should be chosen with the careful consideration of energy conversion process for phase transition.

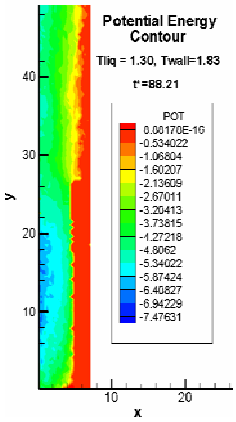

(a-1) $T^*_{sol} = 1.83, T^*_{liq} = 1.30$

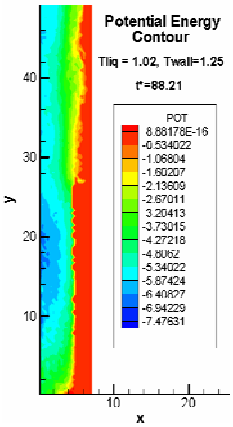

(a-2) $T^*_{sol} = 1.25, T^*_{liq} = 1.02$

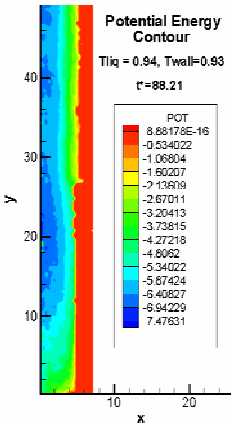

(a-3) $T^*_{sol} = 0.93, T^*_{liq} = 0.94$

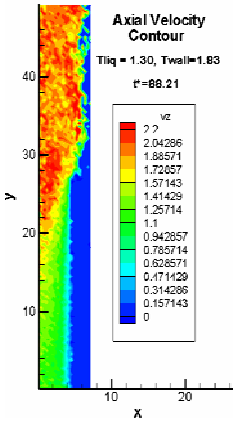

(b-1) $T^*_{sol} = 1.83, T^*_{liq} = 1.30$

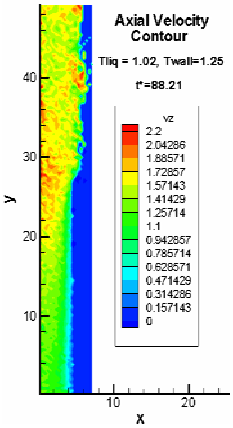

(b-2) $T^*_{sol} = 1.25, T^*_{liq} = 1.02$

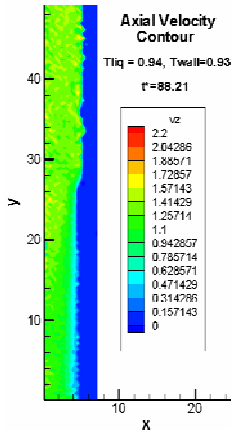

(b-3) $T^*_{sol} = 0.93, T^*_{liq} = 0.94$

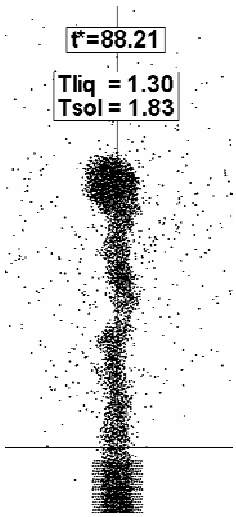

(c-1) $T^*_{sol} = 1.83, T^*_{liq} = 1.30$

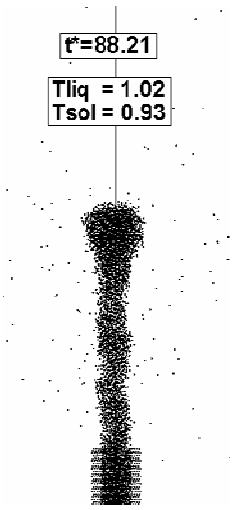

(c-2) $T^*_{sol} = 1.25, T^*_{liq} = 1.02$

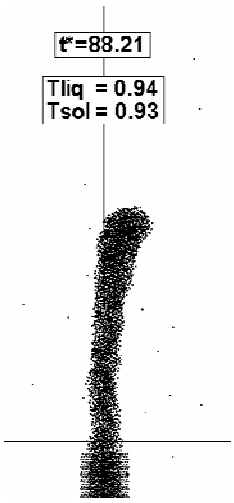

(c-3) $T^*_{sol} = 0.93, T^*_{liq} = 0.94$

Figure 7: 2-D contour and 3-D scatter plots from different temperature conditions.

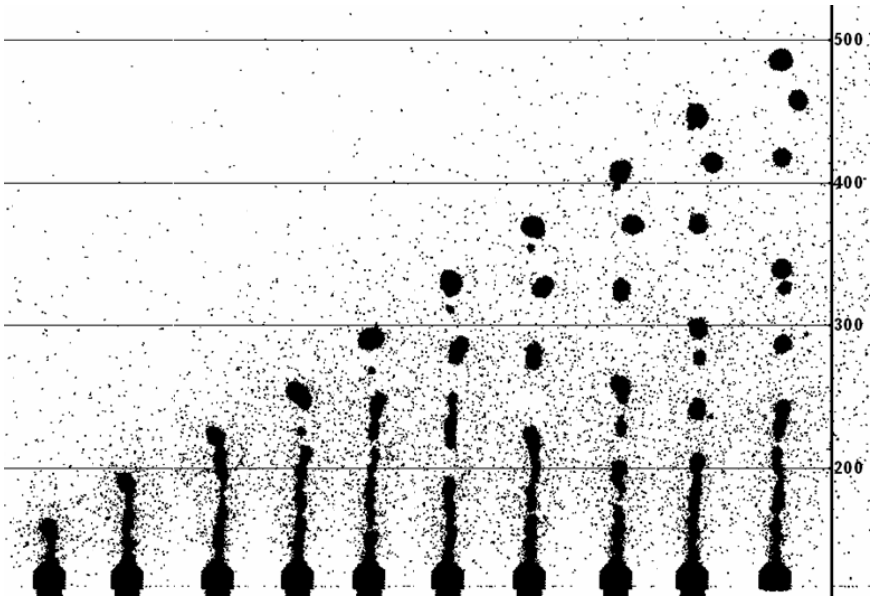

Figure 8: Evolutionary 3-D jet profiles with 45 degree convergent injector. (T_{wall}=1.83, T_{liq}=1.4)

2.4 Sub/supercritical argon nanojet injection

Based on current simulation codes in vacuum condition, the expansion to sub/supercritical condition has been attempted. Our main target in this research project is an adopting MDS as useful numerical tool for understanding complex physics in jet breakup under supercritical condition. However, current tight margin in available numerical capacity is a major obstacle for high pressure calculation. Under very high pressure, the number of gas molecules will exceed that of liquid molecules. Generally the calculation speed is sharply increasing with the increase of number of molecules. To make a matter worse, we also need large chamber volume for gas molecules to minimize the increase of chamber pressure due to vaporized molecules from liquid jet. Therefore we should choose an appropriate trade-off value for chamber size with the careful consideration of calculation time and numerical resources.

First we set the chamber diameter and length as 9 nm and 150 nm respectively. With these dimensions, the number of gas atoms is about 14,000 when pressure is 3 MPa and temperature is 180 K. Another important option for this calculation is how to treat wall boundary. Two different types were tested. First type is all chamber walls are blocked and atoms which collide with wall undergo diffusive reflection. Therefore, total number of gas molecules is fixed during calculation. The other choice is using coaxial injection condition with open chamber end. In this case, molecules can escape from chamber region as well as re-enter chamber. These two tested types are shown in Figure 9. Using molecular-tagging method, molecules in each phase are plotted with different colors. (red: gas, blue: liquid, green: solid).

In non-coaxial case, jet head acted like a ‘piston’ and pushed gas molecules upward. Especially current chamber diameter is comparable to jet head diameter so pressurizing effect can be significant. In our simulation, this pressurizing problem finally leads to sudden burst of liquid jet during simulation. This is highly unphysical so we should increase the chamber diameter substantially to prevent jet burst problem. This was also one of the reasons that we use coaxial gas flow. Under coaxial gas flow condition, gas molecules can be added into chamber region continuously so spatially uniform gas density can be obtained. This coaxial gas jet case is described in Figure 9-(b). For generating continuous gas flow, ‘periodic-shell’ boundary condition was used [5]. Periodic-shell boundary condition can produce continuous gas flow with fixed temperature and density.

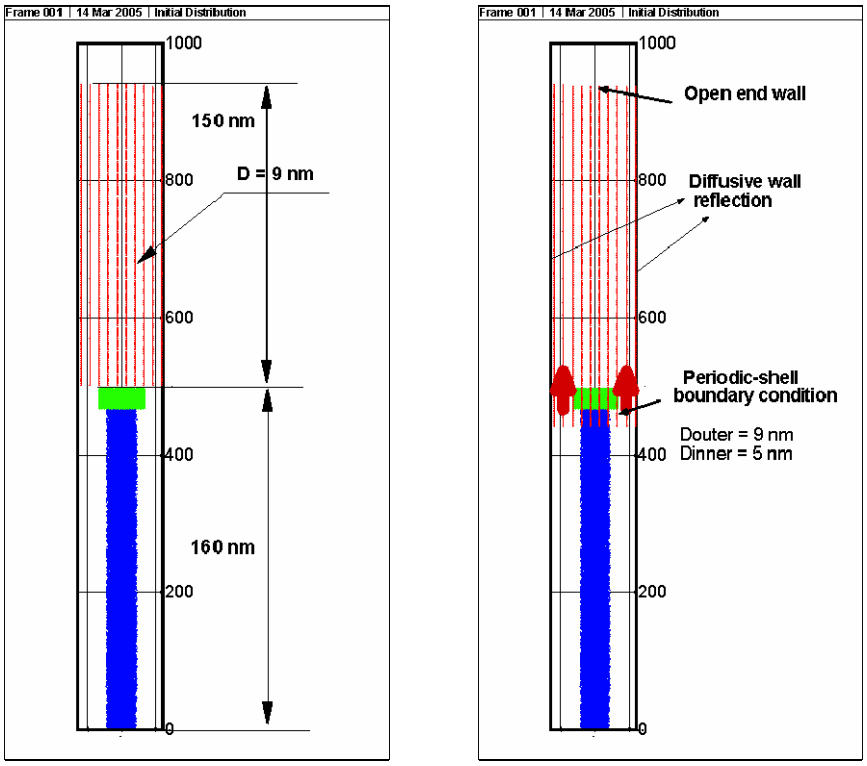

(a) non-coaxial (b) coaxial

Figure 9: Schematics of initial simulation geometries.

	P* (gas)	T* (gas)	Vgas (m/sec)	Dcham (nm)	Status
1	0.919	1.657	240	12	Near critical
2	0.613	1.193	120	9	Intermediate
3	0.613	1.193	120	12	Intermediate
4	0.613	1.193	240	12	Intermediate
5	0.613	1.193	360	12	Intermediate
6	0	0	0	0	Vacuum
7	0.102	1.657	120	12	Subcritical
8	0.102	1.657	240	12	Subcritical
9	0.102	1.657	360	12	Subcritical
10	1.225	1.657	120	12	Supercritical
11	1.225	1.657	240	12	Supercritical
12	1.225	1.657	360	12	Supercritical

Table 2: Tested conditions

With this coaxial gas flow, various simulations were made under sub/supercritical conditions. Comparing to previous vacuum results, there are many new important factors which can elevate the level of complexity in jet breakup mode. For example, high pressure effect and coaxial flow effect can add complexities into the jet breakup characteristics. Therefore we need a variety of simulation cases to examine the effect of various factors. Test cases are shown in Table 2. Pressure and temperature are

in reduced form by its critical values. Pressure and temperature at critical point are 4.897 MPa and 150.86K respectively.

Test case 2 and 3 were chosen to verify the effect of chamber size. However, results from both cases showed significant differences in jet disintegration behavior so 12 nm chamber diameter was used in all the other calculations. From these conditions, it is possible to make rough estimation of subsequent jet breakup regime by using classic jet breakup theory. Generally the jet breakup characteristics can be classified by 3 non-dimensional numbers, Reynolds, Weber and Ohnesorge number. Definitions of these variables are in Eq. 4.

Eq. 4
$$We_L = \frac{U_L^2 \rho_L d_j}{\sigma},\ \mathrm{Re}_L = \frac{\rho_L d_j U_L}{\mu_L},\ Z = \frac{\mu_L}{\sqrt{\rho_L \sigma d_j}} = We_L^{1/2}\,\mathrm{Re}_L^{-1}$$

Weber number is the ratio between kinetic energy of jet and surface tension energy. But, when aerodynamic kinetic energy is dominant like a coaxial jet injection, aerodynamic Weber number is frequently used. Aerodynamic Weber number is in Eq. 5.

Eq. 5
$$We_G = \frac{(U_L - U_G)^2 \rho_G d_j}{\sigma}$$

With these non-dimensional numbers, the regimes of possible jet breakup with given condition can be roughly estimated. This is shown in Figure 10.

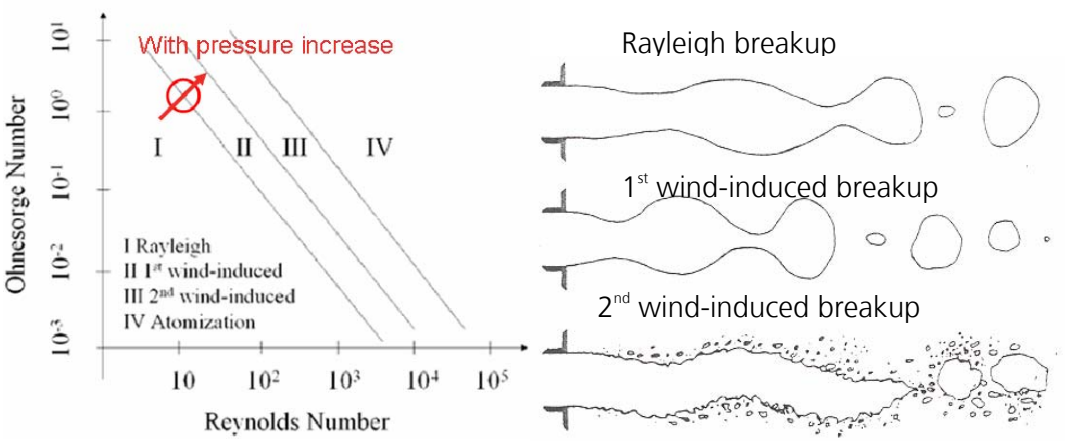

Figure 10: Jet breakup regimes (a) and general jet breakup behaviors (b).

With the assumption that surface tension and viscosity of nanojet would not deviate from those properties from bulk argon liquid, we calculated those non-dimensional numbers. However, our jet diameter is only 3 nm so available magnitude of Reynolds numbers can not exceed the order of 10. Therefore, the only way to reach the 1st wind-induced is the increasing Ohnesorge number (see Figure 10-(a)). Fortunately it is possible by increasing background gas pressure. Generally surface tension is rapidly decreasing with pressure increase. The decrease of surface tension directly leads to the increase of Ohnesorge number so we could expect 1st wind-induced breakup in high pressure cases. We marked the achievable conditions from current simulation in Figure 10-(a) (red circle). Our simulation conditions lay around the interface between Rayleigh and 1st wind-induced breakup.

2.5 Results

2.5.1 3D-slice view

Under high gas pressure, the clear observation of liquid jet is blocked by too many gas molecules around the jet. To get a better observation under high pressure, we truncated very thin 3D slice from central region of system. From this 3-D slice, we calculated the number of neighbor molecules of each atom and made a contour plot. We counted neighbor atoms inside imaginary sphere whose radius is 3.0 σ. This number informs the level of local density as well as 'phase'. Therefore, it is very effective parameter to define unclear phase under high pressure. The details of this procedure are described in Figure 11. For the better observation, we truncated atoms which have neighbor atoms less than 5. Thus, in dilute gas, most of gas atoms are not plotted in slice plot.

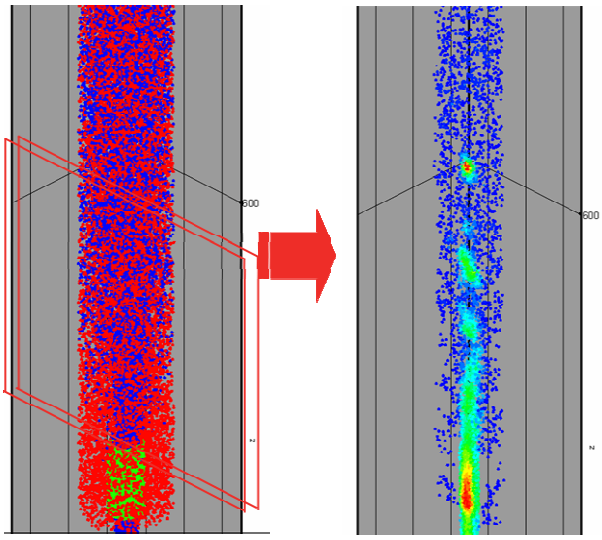

Figure 11: Schematic of slice view plotting method

2.5.2 Subcritical condition (case 7-9)

First test condition is subcritical cases (case 7 to 9) which are expected to have similar breakup characteristics as previous vacuum results. Figure 12 illustrates transient nanojet breakup processes of vacuum and subcritical cases (case 8). Plotting interval is 23.21 non-dimensional time (50 psec) and this plotting interval is used in all other plots. Color of each molecule means the number of neighbor molecules in given atom. As expected before, overall breakup procedures are quite identical.

Remarkable difference is the size of droplet. Subcritical case has larger droplet size due to relatively weaker vaporization of surface atoms. However, the observed droplet size in Figure 12-(a) is slightly underestimated that its real size in 3D scatter plots (see Figure 8) because the center of droplet is not located in the central region. Even though coaxial injection condition was adopted, both liquid jet and coaxial gas flow have identical axial velocity so aerodynamic effect is marginal. To examine the effect of relative velocity difference into jet breakup characteristics, we changed the speed of coaxial gas flow as 120 m/sec and 360 m/sec. These results are shown in Figure 13. Figure 13-(a) shows the results when coaxial gas flow is faster than liquid jet. Due to fast coaxial gas flow, liquid drops drift down the chamber further than the result in Figure 12-(b). Therefore at the end of calculation (t*=306), first droplet reaches further than 900 non-dimensional length. Also, the size of droplet is slight decreased than previous case. However, when the coaxial gas flow is slower than liquid jet, several interesting features were observed. First, it has shortest jet breakup distance. Initial surface disturbances grow very fast and lead to jet breakup. Because of slow gas flow velocity, droplet

penetration distance is much less than high speed gas flow case. This result urges that plus relative velocity between jet and coaxial gas flow ($V_r=V_{jet}-V_{gas}$) is more favorable to decrease nanojet intact length than minus relative velocity.

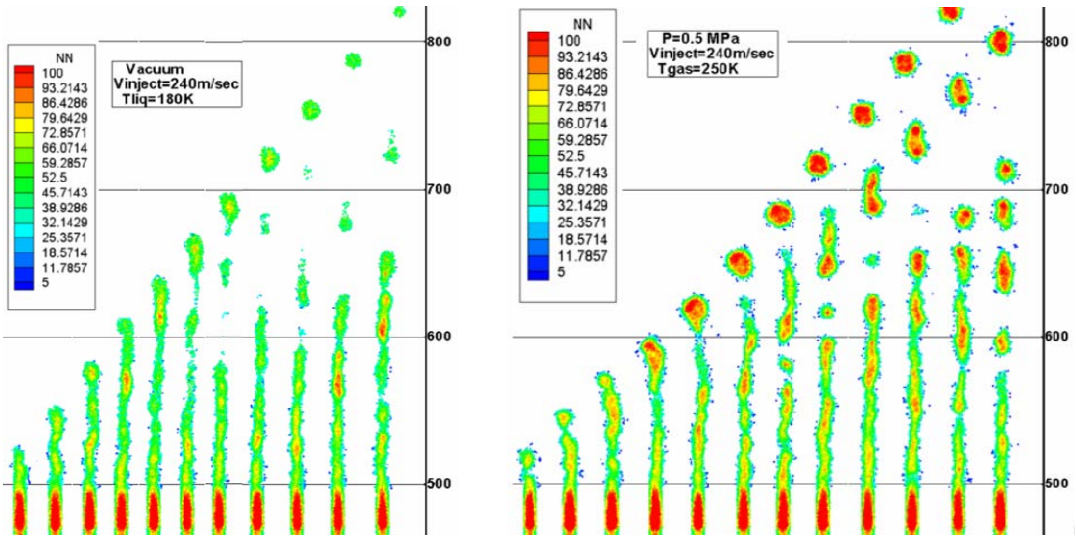

(a) (b)

Figure 12: Transient nanojet breakup profiles, under vacuum (a) and subcritical (case 8)(b) conditions

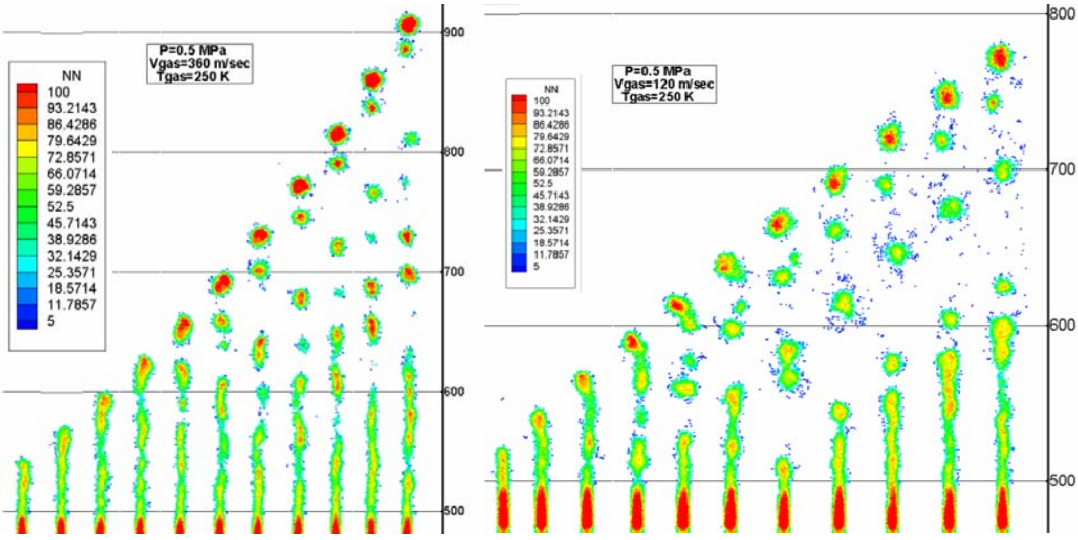

(a) (b)

Figure 13: Transient plots of nanojet breakup process, Vgas=360m/sec (a) Vgas=120m/sec (b)

2.5.3 Near critical conditions (case 1-5)

5 different calculations were made with elevated gas pressure. One is 4.5 MPa (case 1) and the others are 3 MPa (case 2-5). Temporal evolution of jet breakup procedure is in Figure 14. Both cases have no relative velocity between jet and coaxial gas flow. Comparing with previous subcritical results, observed droplet size is smaller. Especially as thermodynamic conditions moves toward critical point, fast droplet vaporization becomes remarkable. In case 1 (Figure 14-(a)), all droplets have been vaporized before reaching 900 non-dimensional distance. This rapid droplet vaporization is mainly due to the decrease of heat of vaporization with pressure increase. However, it is expected that the vaporized atoms could enhance the level of local pressure and density. Therefore, local

thermodynamic condition near the jet surface can approach toward critical condition. The presence of atoms with sky blue color at the periphery of jet surface in Figure 14-(a) means the occurrence of continuous density profile with obscure phase interface. As mentioned before, we expected that the increase of pressure could result in 1st wind-induced breakup. Current results tell us that this expectation is correct. When pressure is increased, first observable change is the decrease of droplet size and the short jet breakup length. Both cases in Figure 14 have relatively shorter jet breakup distance than previous low pressure cases. Observed droplet size is inversely proportional to gas pressure.

In Figure 15, the effect of positive and negative relative velocity into nanojet breakup is shown. Figure 15-(a) and (b) show the results with positive and negative relative velocity respectively. Similar to previous subcritical results, slow coaxial flow (Figure 15-(a)) causes rather larger droplet size with shorter droplet penetration distance. Braking effect of slow coaxial gas jet is intensified under higher gas pressure. Therefore, the penetration length at the end of calculation is much shorter than that of subcritical condition (Figure 13-(b)). Oppositely the blowing effect with negative relative velocity is also augmented with the increase of pressure and this is shown in Figure 15-(b).

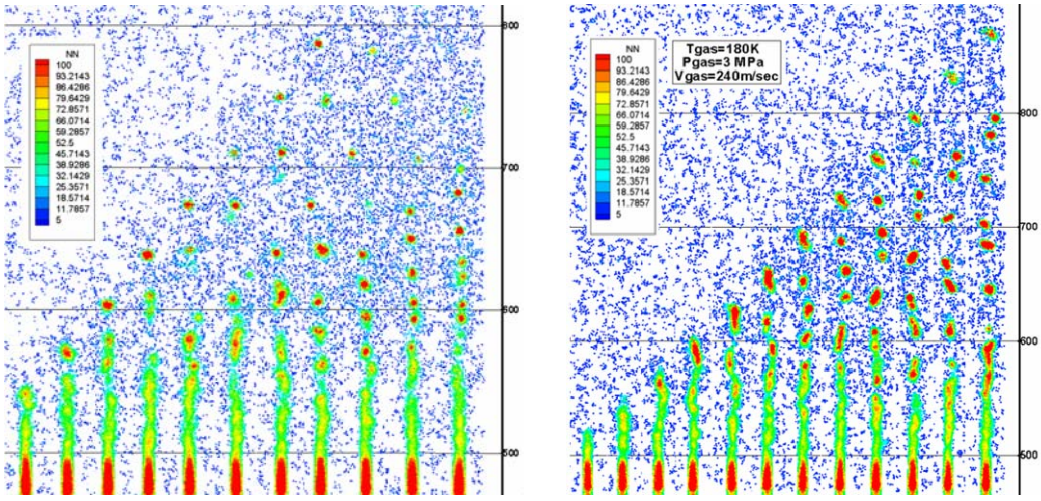

(a) (b)

Figure 14: Transient jet breakup processes at near critical point, case 1 (a) and case 4 (b)

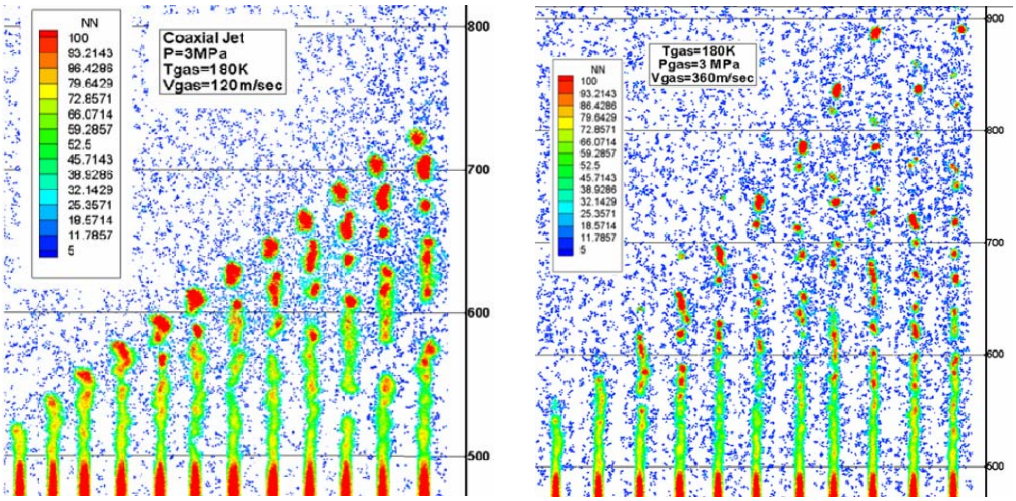

(a) (b)

Figure 15: Transient jet breakup profiles, case-3 (a) and case-5 (b)

2.5.4 Supercritical conditions (case 10-12)

With the elevation of coaxial gas pressure over the critical limit, nanojet injection simulations were made with identical relative velocities as previous calculations. These results are shown in Figure 16 and Figure 17. The result with negligible aerodynamic disturbance is in Figure 16. Both jet and gas flow have identical axial velocity therefore there is very weak contribution of aerodynamic force into jet breakup. In previous results under subcritical conditions, droplets have a distinct phase interface, which is denoted by the non-continuous color change from green to blue. However, under supercritical condition, phase interface of droplet is becoming obscure and the continuous gradation of contour color from red to blue is frequently detected. In addition, due to the substantial decrease of heat of vaporization, droplets are rapidly vaporized. As jet is moving downstream, liquid jet, which was initially at subcritical condition is heated by hot gas flow and reaches critical condition. It is hard to define the droplet diameter but it seems that droplet diameter is smaller than that of subcritical conditions.

Results with non-zero relative velocity are shown in Figure 17. When liquid jet is twice faster than coaxial gas flow (Figure 17-(a)), no droplet is observed except first one. After the initial transient period, jet vaporizes immediately without forming a droplet. Also near jet periphery, continuous density gradient is established. This is a definite evidence of supercritical fluid. Figure 17-(b) shows the results with the positive relative velocity. Due to blowing effect of fast coaxial gas flow, local density around jet periphery is lower than negative relative velocity case. Comparing to the result in Figure 16, the contribution of aerodynamic effect slightly causes smaller droplet diameter.

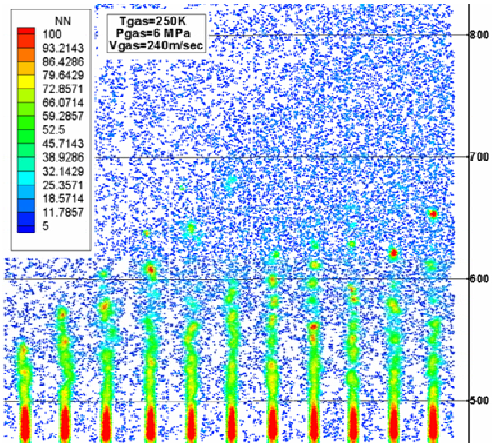

Figure 16: Transient jet breakup profiles under supercritical condition (zero relative velocity)

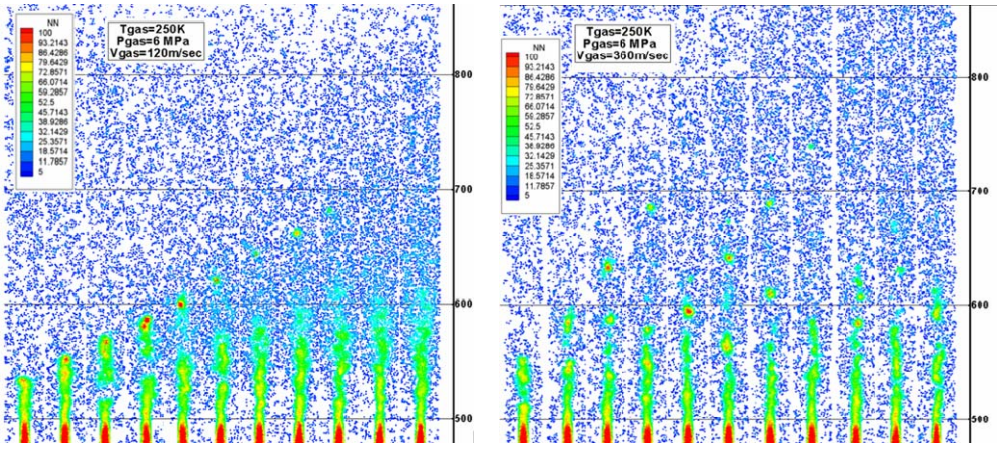

(a) (b)

Figure 17: Transient jet breakup profiles under supercritical condition . (a): negative relative velocity, (b): positive relative velocity

2.6 Concluding Remarks

During the last three years, we have focused the possibility of adopting molecular dynamics method as an effective numerical tool for investigating complicate physics in high-pressure jet breakup behavior. Even though the rapid development of computation power, there is still a definite upper limit of available system size, which currently stays nano-meter scale. Due to this strict restriction in system size in molecular dynamics, three non-dimensional numbers (Re, We, Oh), which defines the jet breakup characteristics cannot be matched between molecular dynamics and experiments. For example, our nanojet diameter is only 3 nm thus available Reynolds number is about 5 to 15. However, the minimum available Reynolds number in our nitrogen capillary jet experiment is generally much higher than this. Therefore, it is not available to make direct quantitative comparison between experiment and simulation at this moment. In spite of this intrinsic matching problem, our simulation results show quite good qualitative agreement with our experiment results. Figure 18 compares the results from current simulations with our experiment results with liquid nitrogen capillary injection (see our previous report [1]). Except Figure 18-(b), qualitative similarities between simulations and experiments were obtained with almost identical reduced pressures. Considering the orderly different system size in experiment and simulations, the similarities in jet breakup characteristics are remarkable. This figure explains us why we need to pay attention to this state of the art numerical method. The range of its application field will be rapidly broadened with the development of computers. We hope our research would be a foundation stone for applying molecular dynamics for macro/mesoscale systems.

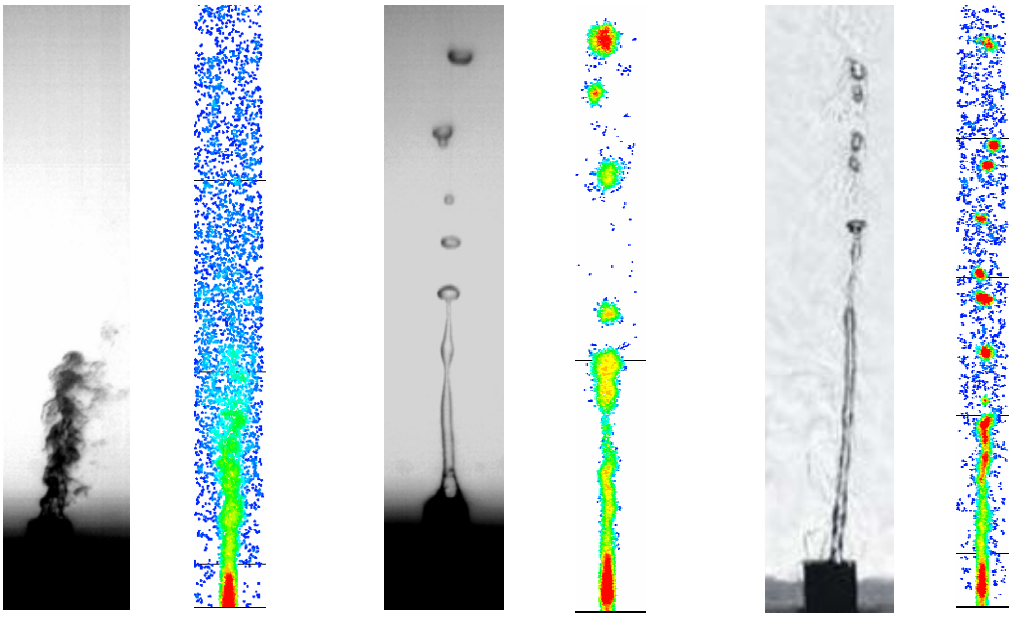

(a-1)	(a-2)	(b-1)	(b-2)	(c-1)	(c-2)
P_r = 1.148	P_r = 1.225	P_r = 0.721	P_r = 0.102	P_r = 0.735	P_r = 0.613
Re=43	Case 10	Re=147	Case 7	Re=335	Case 4

Figure 18: Comparison between experiment results with nitrogen jet and simulation results with argon nanojet. ($T_{r,gas}$ = 2.213 ~ 2.306 : experiment)

3. References

[1] H. Shin, N. Hammou, K. Ludwig, R. Gladulich, S. Ferdousi, G. Schneider, M. Oschwald, Molecular Dynamics Simulation of Supercritical Jets. Interim Report Phase III Item 1, November 2004, DLR-LA-MD-RP-004

[2] Micheal Moseler, Uzi Landman, Formation, Stability and Breakup of Nanojets, Science Vol. 289, 2000

[3] F. Datchi, P. Loubeyre, R. LeToullec, Melting Curves of Hydrogen, H_2O, Helium and Argon at High Pressure, ICTP Science Abstract No. 37, Adriatico Research Conference Simple System at high pressure and temperatures: Theory and Experiments, Miramare-Trieste, Italy 1-4 July 1997

[4] Kenichiro Koga, G. T. Gao, Hideki Tanaka, X. C. Zeng, Formation of Ordered Ice Nanotubes inside Carbon Nanotubes, Nature 412 pp 802-805, 2001

[5] Y. Maniwa, H. Kataura, M. Abe, A. Udaka, S. Suzuki, Y. Achiba, H. Kira, K. Matsuda, H. Kadowaki, Y. Okabe, Ordered Water inside Carbon Nanotubes: Formation of Pentagonal to Octagonal Ice-nanotubes, Chem. Phys. Lett. 401 pp 534-538, 2005

[6] Akira Satoh, Periodic-shell Boundary Condition for Soft Molecular Systems: Molecular Dynamics Simulations of Flow Past a Circular Cylinder, Molecular Physics, vol. 92, No. 4, pp. 715-721,1997